Arab J. Nucl. Sci. Appl., Vol. 55, 1, 147 -158 (2022)

ISSN 1110-0451

Arab Journal of Nuclear Sciences and Applications

Web site: ajnsa.journals.ekb.eg

(E S N S A)

The Structure, and Magnetic Properties of $NiR_{0.05}Fe_{1.95}O_4$ (Rare Earth R=Sm, Gd): Effect of Thermal Neutron Radiation

Kh. Roumaih, M. Yehia*, and S.M. Ismail

Reactor Physics Department, Nuclear Research Center, Egyptian Atomic Energy Authority, Cairo, Egypt

ARTICLE INFO

Article history:

Received: 13th July 2021

Accepted: 1st Nov. 2021

Keywords:

Rare Earth Ferrites,
Thermal Neutron Exposure,
Elastic Properties,
XRD,
Saturation Magnetization.

ABSTRACT

The structural, elastic, and magnetic properties of $NiR_{0.05}Fe_{1.95}O_4$ (R= Sm, and Gd) spinel ferrites were studied before, and after thermal neutron exposure. Polycrystalline $NiFe_{1.95}Gd_{0.05}O_4$, and $NiFe_{1.95}Sm_{0.05}O_4$ ferrites were synthesized using the standard ceramic method. The samples were irradiated by thermal neutrons using a rabbit system for 2 and 8 seconds with doses of 2.3 and 7.8 Gy, respectively. X-ray powder diffraction (XRD) revealed the formation of the cubic spinel phase with a secondary phase of $RFeO_3$. XRD measurements indicated that by increasing the thermal neutron dose, the crystallinity of the prepared samples increases and the lattice parameter decreases. Fourier-transform infrared (FTIR) spectroscopy was utilized to examine the elastic properties, whereas, the elastic moduli and Debye temperature were obtained. Using a vibrating sample magnetometer (VSM), the effect of thermal neutron exposure on the magnetic properties was investigated. The saturation magnetization (M_s) increased by increasing the thermal neutron dose. The structure, elastic and magnetic parameters dependence on the thermal neutron dose may suggest that thermal neutron exposure can be used to fine-tuning these properties for particular applications.

1. INTRODUCTION

In the past few years, there has been an increase in the demand for microwave devices in automotive, consumer, and industrial radar systems to reduce the cost of the device [1–3]. Spinel ferrites are considered to be the best material for microwave absorbers because of their stability, high electrical resistivity, high magnetization, and high Curie temperature [1, 4]. Doping of ferrites by traces of rare earth elements modifies the structure and consequently changes its basic properties, rendering them useful in a variety of applications [5-10]. The magnetic moments of R ions vary from 0 (La^{3+}) to 10.5μB (Dy^{3+}) and therefore they interestingly can be isotropic or anisotropic in relation to the variation in the f electron orbital contribution to magnetic interactions [11].

Nickel ferrites is an interesting family of ferrites and has been widely used in various electronic devices because of its chemical stability, large permeability at high frequency, high electrical resistivity, and cost-effectiveness [12]. Nickel ferrite crystallizes in a fully inverse spinel structure, which contains two different cation sites: eight tetrahedral (A) sites completely occupied by Fe^{3+} ions and 16 octahedral [B] sites equally occupied by both Ni^{2+} ions and Fe^{3+} ions [11].

For rare earth doped ferrites, frequent difficulties were reported in synthesizing a single-phase compound. The R^{3+} ions have a significantly larger ionic radius compared to that of Fe^{3+} ions. Therefore, they diffuse to the grain boundaries of the spinel network even for very low R content. Such behavior causes the precipitation of extra amorphous or crystalline phases like orthoferrites ($RFeO_3$) [13-16]. In a previous study, single phase $NiFe_{1.99}R_{0.01}O_4$ (R = Sm, Gd, Eu, La) samples were successfully prepared using the standard ceramic method [11]. Mössbauer effect measurements referred that R^{3+} ions substituted Fe^{3+} ions in the octahedral B site. Vibrating sample magnetometer

Corresponding author: m6yehia@yahoo.com
DOI: 10.21608/ajnsa.2021.86106.1486

measurements indicated an increase in the coercivity and saturation magnetization for all doped samples and the highest saturation magnetization was obtained for Gd and Sm-doped Ni-ferrite samples [11].

However, the study of the effect of thermal neutrons radiation on the physical properties of ferrite is rarely reported [17,18]. Neutron irradiation can be a powerful tool to increase crystallographic defects to modify the structural, electrical, and magnetic properties of ferrites.

In the present work, $NiR_{0.05}Fe_{1.95}O_4$ (R=Sm and Gd) compounds were prepared using the standard ceramic method. The effect of thermal neutron exposure on structural, elastic, and magnetic properties of these rare earth doped nickel ferrites was systematically studied using X-ray powder diffraction, Fourier-transform infrared spectroscopy (FTIR), and vibrating sample magnetometer (VSM) measurements.

2. Experimental

2.1 Materials and methods

$NiR_{0.05}Fe_{1.95}O_4$ (R=Sm, and Gd) compounds were prepared by a solid state reaction using NiO, Fe_2O_3, R_2O_3 (R=Sm and Gd) with purity of 99.999 % as starting materials. The reaction can be described as:

$$NiO + (0.975)\, Fe_2O_3 + (0.025)\, R_2O_3 \xrightarrow{yields} NiFe_{1.95}R_{0.05}O_4$$

The oxides of each sample with stoichiometric ratios were mixed and ground to a very fine powder. Later, the powders were presintered at 1250 °C for 48 hr and then slowly cooled. The mixture of each sample is reground again, pressed into disc form, and finally sintered at 1300 °C for 10 hr and then slowly cooled to room temperature. The prepared samples were exposed to thermal neutrons using a rabbit system for 2 and 8 seconds at ET-RR2 Reactor, Nuclear Research Center, Egyptian Atomic Energy Authority. The thermal neutrons had an energy of 0.025 eV and a flux equal to 10^{11} (n.cm^{-2}.sec^{-1}). The masses of the samples exposed to thermal neutrons for 2 sec. and 8 sec. were 1 and 1.18 gram, respectively. The absorbed doses were calculated as [19,20]:

$$dose = \frac{(flux)\,(conversion\ factor)(irradiation\ time)}{mass} \quad (1)$$

The conversion factor for thermal neutron with energy 0.025 is 4.14×10^{-3} (mrem.h^{-1} per n.cm^{-2}.sec^{-1}) [19,20]. The absorbed doses for 2 sec. and 8 sec are 2.3 and 7.8 Gy, respectively. Table 1 illustrates the prepared samples, doses, and the used abbreviations.

Table (1): Abbreviations of the studied samples

Sample	Dose (Gray)	Abbreviations
$NiFe_{1.95}Sm_{0.05}O_4$	0	SmZ0
	2.3	SmZ2
	7.8	SmZ8
$NiFe_{1.95}Gd_{0.05}O_4$	0	GdZ0
	2.3	GdZ2
	7.8	GdZ8

2.2 Characterization

The crystal structure and phase purity of the samples were studied by X-ray powder diffraction technique; Philips X'pert multipurpose diffractometer with CuK_α radiation (λ = 1.5418 Å). Fourier transform infrared spectra of different samples were recorded using (Spectrum 100; Perkin Elmer, USA) in the spectral range of 800–400 cm^{-1}. Magnetic measurements were carried out using a vibrating sample magnetometer VSM (9600-1 LDJ, USA) with an applied magnetic field up to 20 kG at room temperature.

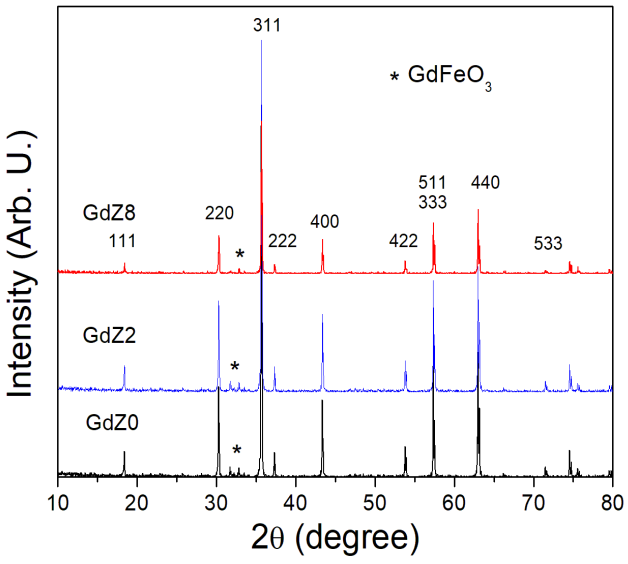

Fig. (1): XRD patterns of $NiFe_{1.95}Gd_{0.05}O_4$ ferrites at different doses

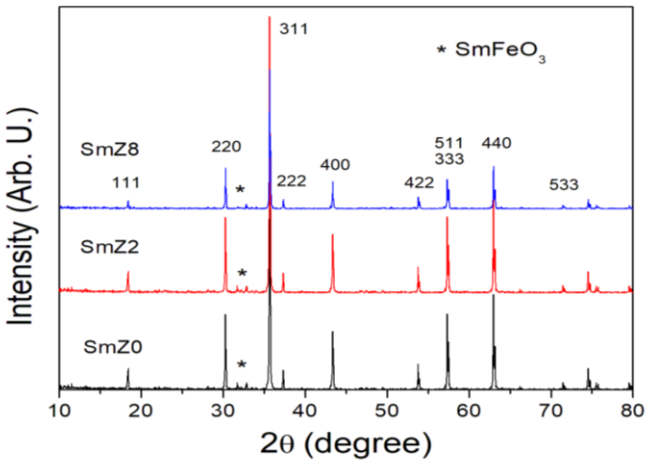

Fig. (2): XRD patterns of $NiFe_{1.95}Sm_{0.05}O_4$ ferrites at different doses

3. RESULTS AND DISCUSSION

3.1. XRD measurements

Figures 1 and 2 show the XRD patterns for the synthesized $NiFe_{1.95}Gd_{0.05}O_4$ and $NiFe_{1.95}Sm_{0.05}O_4$ samples, respectively, before and after thermal neutron exposure. The formation of the cubic spinel structure was confirmed by the observation of the diffraction peaks indexed to the spinel phase with space group Fd-3m [12,13]. However, secondary peaks in the 2θ range from 30 to 35 appear with a minor amount of ortho-ferrite phases of $GdFeO_3$ and $SmFeO_3$ [14]. Interestingly, the intensity of the secondary peaks relative to spinel phase peaks decreases with increasing the exposure time and consequently the absorbed dose. As mentioned before, the ionic radius of the rare earth ions is much larger than that of the Fe^{3+} ions. The ionic radius of the Fe^{3+} ion in the octahedral site is only $r(Fe^{3+})$= 0.645 Å, whereas, for Gd^{3+} and Sm^{3+} ions, $r(Gd^{3+})$= 0.938 Å and $r(Sm^{3+})$=0.958 Å, respectively [15]. Such a significant deference interrupts the spinel structure and causes the formation of the ortho-ferrite phases [16,21,22].

Table (2): The lattice parameters *a*, the particle size (*D*) calculated from W-H plot, microstrain (*ε*) of $NiGd_{0.05}Fe_{1.95}O_4$, and $NiSm_{0.05}Fe_{1.95}O_4$ ferrites at different doses

	$NiFe_{1.95}Sm_{0.05}O_4$			$NiFe_{1.95}Gd_{0.05}O_4$		
	SmZ0	**SmZ2**	**SmZ8**	**GdZ0**	**GdZ2**	**GdZ8**
***a* (Å)**	8.345	8.34	8.32	8.411	8.34	8.28
ρ_x						
D (nm)	88	241	170	169	161	693
***ε* (Å)10^{-4}**	2.31	10.08	7.98	9.68	9.3	15.2

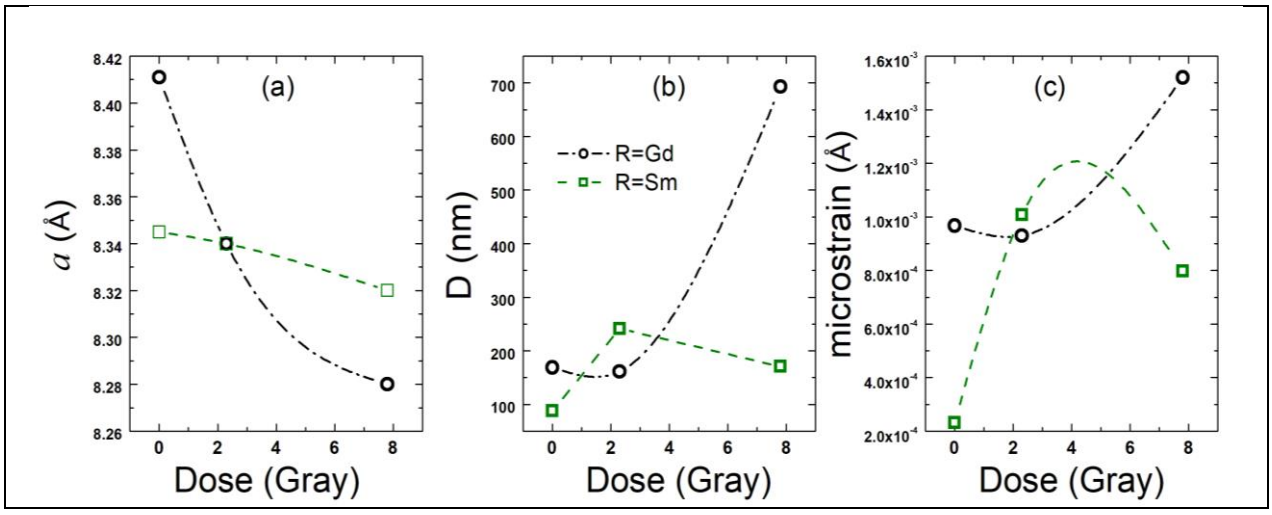

Fig. (3): a) The lattice parameter *a*, b) The particle size D calculated from W-H plots, c) Microstrain ε of $NiFe_{1.95}Gd_{0.05}O_4$ and $NiFe_{1.95}Sm_{0.05}O_4$ ferrites at different doses

The lattice constant (a) was calculated from Miller indices of the crystal planes (h, k, and l) and the interplanar distance (d) using the equation:

$$a = d\ (h^2 + k^2 + l^2)^{\frac{1}{2}} \qquad \textbf{(2)}$$

As indicated in Table (2) and Figure (3a), the lattice constant decreases with increasing the exposure doses, and the effect of the exposure dose is more pronounced for $NiGd_{0.05}Fe_{1.95}O_4$ samples. Such behavior is accompanied by the decrease of the width of the diffraction peaks with increasing the dose. The broadening of XRD peaks (β) is related to the crystallite size and lattice strain, and can be formulated as [23]:

$$\beta = \frac{\lambda k}{D\ cos\theta} + 4\varepsilon\ tan\theta \qquad \textbf{(3)}$$

where λ is the XRD wavelength (CuK_α radiation with λ = 1.5418), k=0.9, ε microstrain, and D particle size. In this case, the Williamson and Hall plot can be drawn from the equation:

$$\beta\ cos\theta = \frac{\lambda k}{D} + 4\varepsilon\ sin\theta \qquad \textbf{(4)}$$

The Williamson and Hall plot was obtained using the (2 2 0), (3 1 1), and (4 0 0) peaks.

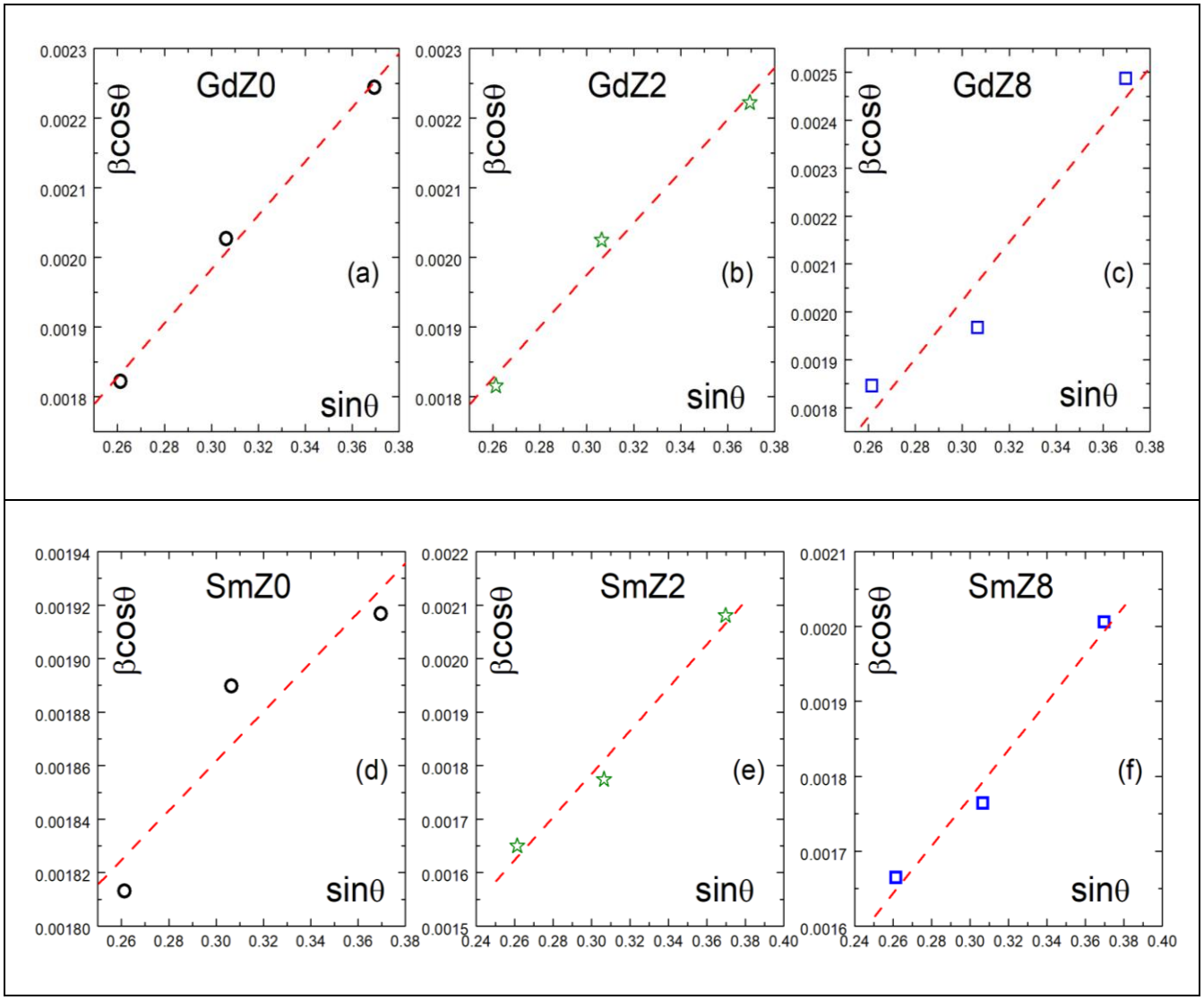

Fig. (4): W-H plots at different doses: a,b,c) $NiFe_{1.95}Gd_{0.05}O_4$ and d,e,f) $NiFe_{1.95}Sm_{0.05}O_4$ ferrites

The estimated particle size and strain values of $NiFe_{1.95}Gd_{0.05}O_4$ and $NiFe_{1.95}Sm_{0.05}O_4$ samples at different doses are summarized in Table (2) and Figure (3). As observed before in the lattice parameter, the effect of the thermal neutron exposure is significantly stronger on the particle size of the $NiFe_{1.95}Gd_{0.05}O_4$ compound, where D($NiFe_{1.99}Gd_{0.01}O_4$) slightly decreases for the GdZ2 sample and then dramatically increases for the GdZ8. On the other hand, D($NiFe_{1.95}Sm_{0.05}O_4$) slightly increases for the SmZ2 sample and later decreases for the SmZ8. This behavior, along with the decrease of the secondary phase peaks, may suggest that the crystallinity of the studied samples is increasing with increasing the thermal neutron exposure dose, especially for $NiFe_{1.95}Gd_{0.05}O_4$. In this case, the energy absorbed by the samples due to thermal neutrons exposure tends to support the incorporation of Gd^{3+} and Sm^{3+} ions in the Ni-ferrite spinel lattice, which might explain the decreased values of *a* by increasing the exposure dose. The stronger effect of the thermal neutron on the $NiFe_{1.99}Gd_{0.01}O_4$ sample can be related to the fact that Gd ions has higher thermal neutrons capture cross section than that of Sm ions [24]. As for the microstrain, ε follows the same behavior of the particle size. ε($NiFe_{1.95}Gd_{0.05}O_4$) slightly decreases for the GdZ2 sample and then increases for the GdZ8. ε ($NiFe_{1.95}Sm_{0.05}O_4$) strongly increases for the SmZ2 sample and later decreases for the SmZ8.

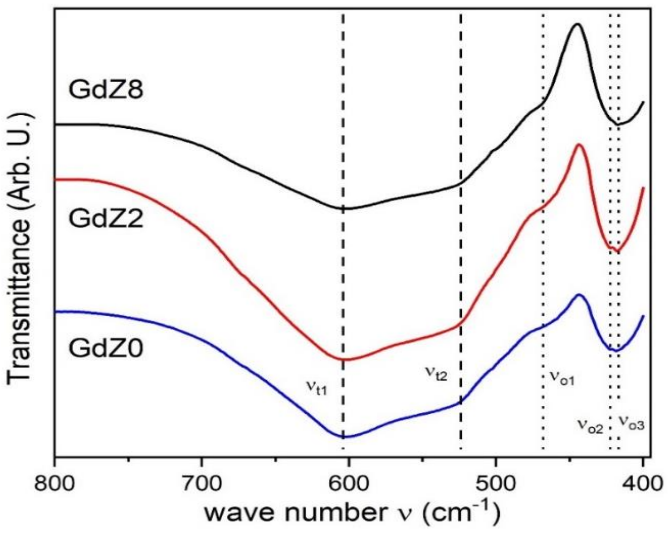

Fig. (5): FTIR measurements of $NiFe_{1.95}Gd_{0.05}O_4$ ferrite at different doses

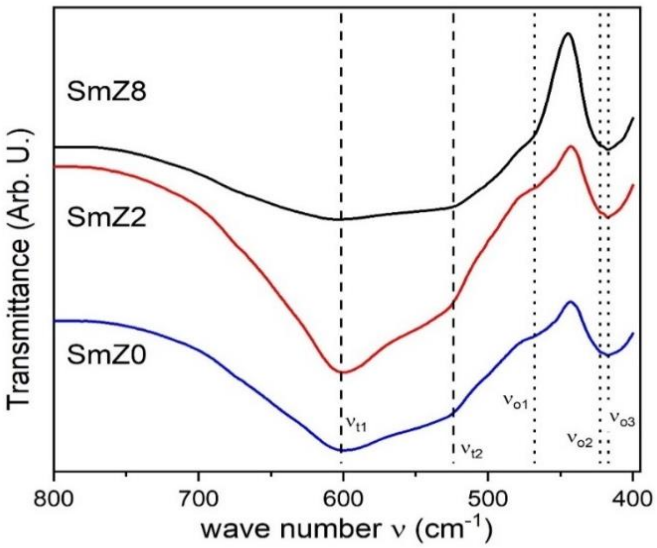

Fig. (6): FTIR measurements of $NiFe_{1.95}Sm_{0.05}O_4$ ferrite at different doses

3.2 Fourier-transform infrared (FTIR) spectroscopy

Figures 5 and 6 show the FTIR spectra of $NiFe_{1.95}Gd_{0.05}O_4$ and $NiFe_{1.95}Sm_{0.05}O_4$ samples before and after thermal neutron exposure within the range from 400 to 800 cm^{-1}. Two bands of vibrational frequencies were observed for all the measured samples. The ν_{t1}, ν_{t2} are assigned to the vibrational modes at the tetrahedral A-site, whereas, ν_{o1}, ν_{o2}, and ν_{o3} are associated with the vibrational modes at the octahedral B-site. Generally, spinel ferrites have two characterized FTIR bands, ν_t and ν_o, associated with the vibrations of the bond between oxygen ion sites of cation sites in both tetrahedral (A) and octahedral (B) sites, respectively [25-27]. The energy required to stretch (cation–Oxygen) bond at the B-site is smaller than that of A-site since the bond length at the octahedral site is longer than that of the tetrahedral site [28,29]. Therefore, the tetrahedral vibrational band is higher than the octahedral band ($\nu_t > \nu_o$). In addition, different atoms with atomic masses (in our case Fe, Ni, Sm, and Gd) will logically have different vibrational frequencies. Another important factor is the correlation between A-site complexes and the B-site [28]. For these reasons, more than one vibrational frequency was observed in both sites in the present compounds. The obtained vibrational frequencies are listed in Table 3. The observed values of ν_{t1}, ν_{t2}, ν_{o1}, ν_{o2} and ν_{o3} for different $NiFe_{1.95}Gd_{0.05}O_4$ and $NiFe_{1.95}Sm_{0.05}O_4$ samples

show weak dependence on thermal neutron exposure. The shift of ν_{o1} frequency for GdZ8 and SmZ8 is higher than any other modes. As observed in the XRD measured, the change in the ν_{o1} frequency of GdZ8 is higher than that of SmZ8. The force constants for the A- and B- sites (k_t and k_o, respectively) can be calculated from [30]:

$$k_t = 7.62 \times M_A \times \nu_t^2 \times 10^{-7}\ N/m \quad \textbf{(5)}$$

$$k_o = 10.62 \times \frac{M_A}{2} \times \nu_o^2 \times 10^{-7}\ N/m \quad \textbf{(6)}$$

In this context, M_A and M_B are the average molecular weights of the cations in tetrahedral and octahedral sites. As mentioned before, Ni-ferrite is fully inversed spinel ferrite and the R^{3+} ions, due you to the large ionic radius, set on the octahedral sites. Hence, the cation distribution $(Fe)_A[NiFe_{0.95}R_{0.05}]_BO_4$ was considered to calculate M_A and M_B. The calculated values of the different force constants are listed in Table (3), whereas, the average force constant k_{tav} and k_{oav} are shown in Figure (7).

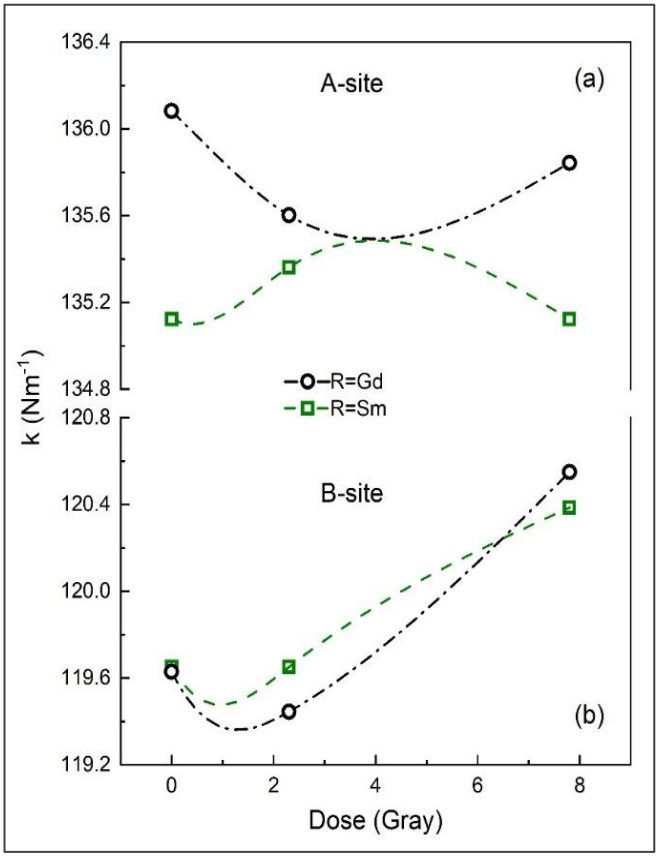

Fig. (7): The dose dependence of the average force constant of $NiFe_{1.95}Gd_{0.05}O_4$ and $NiFe_{1.95}Sm_{0.05}O_4$ ferrites: a) k_{tav} and b) k_{oav}

The ($Cation_A$- O) bond is shorter than ($Cation_B$- O) bond and consequently, the bond in the tetrahedral site is stronger than that in the octahedral site. Therefore, the force constant of the A-site (k_t) is larger than that of the B-site (k_o). The force constant depends on the bond length, charge, mass, and size of the ions forming these bonds. The force constants show weak dependence on exposure dose. The effect of thermal neutron exposure is more pronounced in the B-sites (where the R^{3+} ions). The bulk modulus (B) presents the average stiffness and can be determined as:

$$\mathrm{B} = \frac{\mathrm{k}}{a} \quad \textbf{(7)}$$

Where a is the lattice constant obtained from the XRD measurements. Different elastic parameters can be calculated as [27-32]:

The longitudinal velocity of elastic waves (V_l) $$v_l = [\frac{9B}{5\rho_x}]^{\frac{1}{2}} \quad \textbf{(8)}$$

The transverse velocity of elastic waves (V_t) $$v_t = [\frac{3B}{5\rho_x}]^{\frac{1}{2}} \quad \textbf{(9)}$$

The mean velocity of elastic waves (V_m) $$v_m = \left[\frac{1}{3}\left(\frac{2}{v_t^3} + \frac{1}{v_l^3}\right)\right]^{\frac{-1}{3}} \quad \textbf{(10)}$$

The rigidity modulus (G) $$G = \rho_x v_t^2 \quad \textbf{(11)}$$

Young's modulus (E) $$E = \frac{9\mathrm{BG}}{3\mathrm{B} + \mathrm{G}} \quad \textbf{(12)}$$

The lattice energy (U) $$\mathrm{U} = -3.108\ (M v_m) \times 10^{-12} \quad \textbf{(13)}$$

The values of the longitudinal (V_l), transverse (V_t), and mean (V_m) velocity are summarized in Table (3). As indicated in Figure (8a), the dose dependence of the mean (V_m) velocity is more pronounced for $NiFe_{1.95}Gd_{0.05}O_4$ irradiated samples. V_m decreases gradually for the two compounds.

The calculated values of the elastic parameters; B, G, and E are listed in table 3 and shown in Figure (9). For both $NiFe_{1.95}Gd_{0.05}O_4$ and $NiFe_{1.95}Sm_{0.05}O_4$ compounds, B, G, and E increase slightly and gradually with increasing the thermal neutron dose. Such increase can be attributed to the decrease of the lattice parameter *a* and the increase of the particle size of the studied samples with increasing the thermal neutron dose. The relation between the rigidity modulus (G) and Young's modulus (E) is linear and the slope of this line illustrates the Poisson ratio (σ).

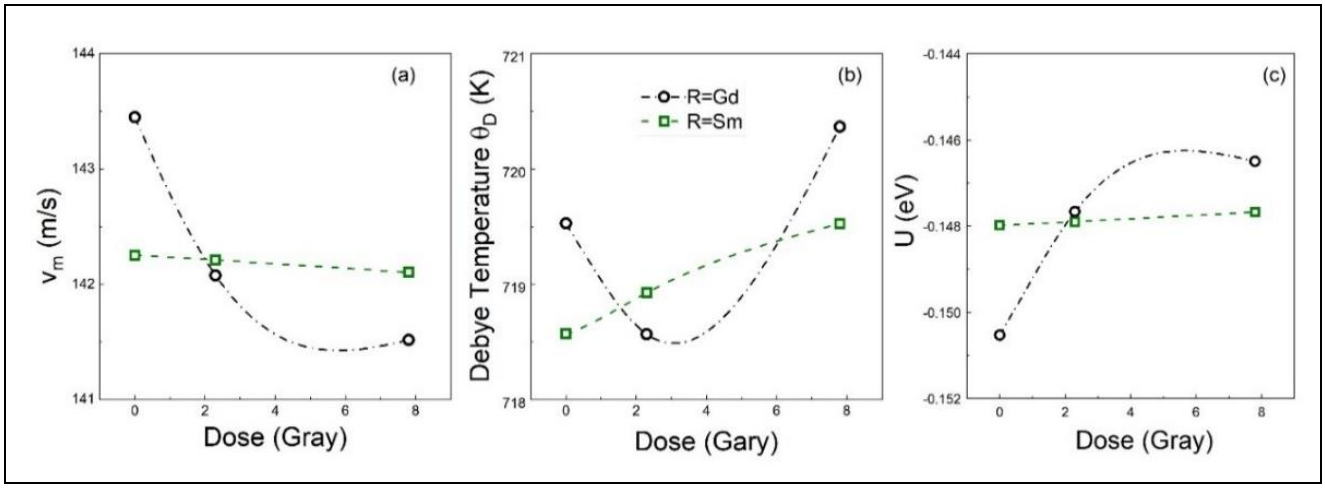

Fig. (8): The dose dependence: a) mean velocity of elastic waves ((V_m), b) The Debye temperature (θ_D), c) The lattice energy (U) of different elastic parameters of $NiFe_{1.95}Gd_{0.05}O_4$ and $NiFe_{1.95}Sm_{0.05}O_4$ ferrites

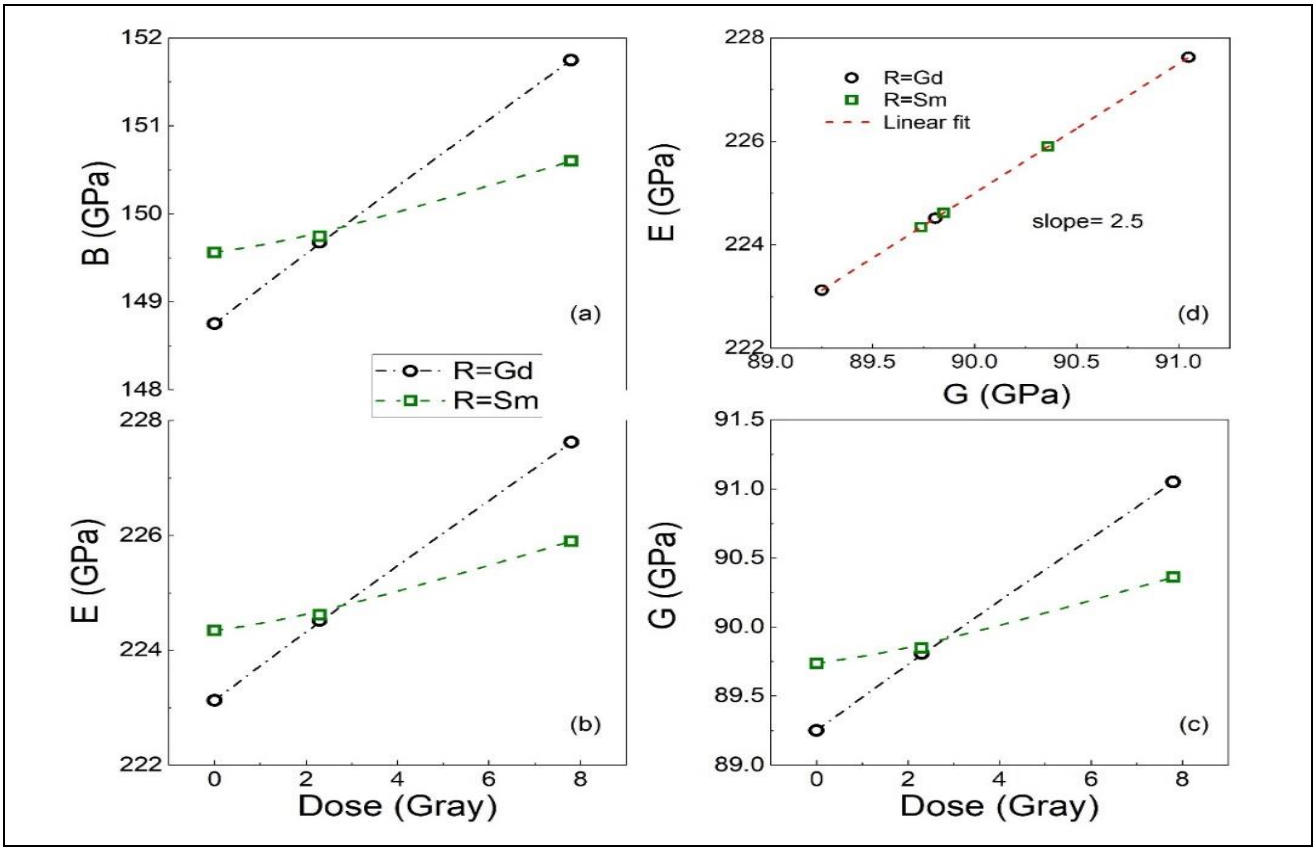

Fig. (9): The dose dependence of different elastic parameters of $NiFe_{1.95}Gd_{0.05}O_4$ and $NiFe_{1.95}Sm_{0.05}O_4$ ferrites: a) Bulk modulus (B), b) Young's modulus c) The rigidity modulus (G). d) The relation between G and E and the value of Poisson ratio=2.5 is indicated.

The Debye temperature (θ_D) is related to the lattice vibration and hence can influence the elastic parameters. According to the Waldron method, the Debye temperature (θ_D) is calculated from the vibration frequency as [30]:

$$\theta_{DW} = \frac{hcv_{av}}{k} \qquad \textbf{(13)}$$

where h is Planck's constant, c is the velocity of light and k_B is the Boltzmann constant. As shown in figure 8b, for $NiFe_{1.95}Gd_{0.05}O_4$, the Debye temperature slightly decreases for the GdZ2 sample and the increase for higher exposure dose (GdZ8). Whereas, for $NiFe_{1.95}Sm_{0.05}O_4$ samples exposed to thermal neutrons θ_D slightly increases. Such behavior illustrates that by increasing the exposure dose, $NiFe_{1.95}Gd_{0.05}O_4$ and $NiFe_{1.95}Sm_{0.05}O_4$ crystals become stiffer [31]. The values of U increase by increasing the exposure dose, whereas the effect is stronger on the Gd doped N-ferrite (figure 8c). The observed increase of U cannot be related to the decreased lattice parameter *a*. The decrease of *a* (from the XRD measurements) will decrease interatomic spacing and lead to shortening of bond lengths, hence the U would decrease [32]. However, the decreased values of the lattice energy with increasing the exposure dose can be attributed to the increase of the elastic parameters and the enhanced particle size [25,32]. As mentioned before, the $NiFe_{1.95}Gd_{0.05}O_4$ compound is more sensitive to thermal neutron exposure than the $NiFe_{1.95}Sm_{0.05}O_4$ compound, which is reflected in the changes in the elastic properties of the two compounds.

Table (3): Tetrahedral and octahedral vibrational frequencies (ν_{t1}, ν_{t2}, ν_{tav}, ν_{o1}, ν_{o2}, ν_{o3}, and ν_{oav}), force constants (k_{t1}, k_{t2}, k_{tav}, k_{o1}, k_{o2}, k_{o3}, and k_{oav}), Bulk modulus (B), longitudinal (V_l), transverse (V_t) and mean (V_m) velocity of elastic waves, Young's modulus (E), the rigidity modulus (G), Debye temperature (θ_D), and the lattice energy (U) of $NiFe_{1.95}Gd_{0.05}O_4$, and $NiFe_{1.95}Sm_{0.05}O_4$ samples before and after thermal neutron exposure

		$NiFe_{1.95}Sm_{0.05}O_4$			$NiFe_{1.95}Gd_{0.05}O_4$		
		SmZ0	**SmZ2**	**SmZ8**	**GdZ0**	**GdZ2**	**GdZ8**
A-site	ν_{t1} (cm^{-1})	600	600	603	603	602	603
	ν_{t2} (cm^{-1})	527	528	524	528	527	527
	ν_{tav} (cm^{-1})	563.5	564	563.5	565.5	564.5	565
B-site	ν_{o1} (cm^{-1})	464	464	469	462	461	467
	ν_{o2} (cm^{-1})	423	422	422	422	422	422
	ν_{o3} (cm^{-1})	417	418	417	418	418	418
	ν_{oav} (cm^{-1})	434.7	434.7	436	434	433.7	435.7
k(A-site)	k_{t1} (Nm^{-1})	153.19	153.19	154.73	154.73	154.22	154.73
	k_{t2} (Nm^{-1})	118.18	118.63	116.84	118.63	118.19	118.19
	k_{tav} (Nm^{-1})	135.12	135.36	135.12	136.08	135.60	135.84
k(B-site)	k_{o1} (Nm^{-1})	136.35	136.34	139.3	135.56	134.98	138.51
	k_{o2} (Nm^{-1})	113.31	112.78	112.78	113.11	113.11	113.11
	k_{o3} (Nm^{-1})	110.12	110.65	110.12	110.97	110.97	110.97
	k_{oav} (Nm^{-1})	119.65	119.65	120.39	119.63	119.45	120.55
B (GPa)		149.56	149.75	150.6	148.75	149.68	151.75
V_l (m/s)		221.93	221.87	221.70	223.8	221.7	220.78
V_t (m/s)		128.13	128.1	128	129.21	127.98	127.47
V_m (m/s)		142.25	142.21	142.10	143.45	142.08	141.52
G (GPa)		89.74	89.85	90.36	89.25	89.81	91.05
E (GPa)		224.34	224.62	225.9	223.13	224.52	227.62
θ_D (K)		718.6	718.9	719.5	719.5	718.6	720.4

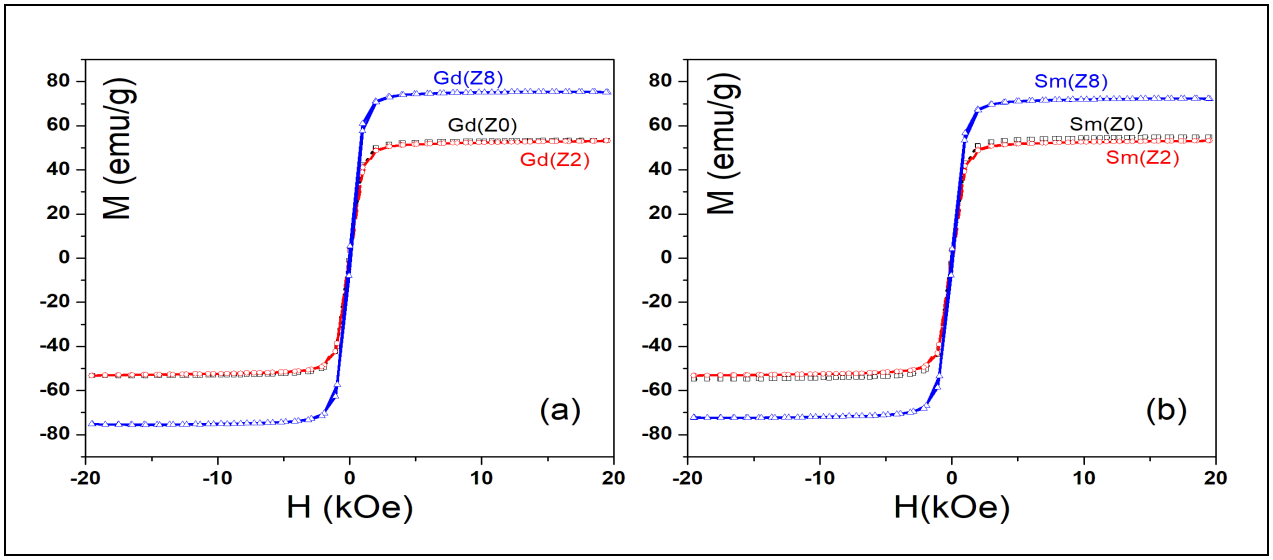

Fig. (10): Room temperature hysteresis loops of a) $NiFe_{1.95}Gd_{0.05}O_4$ and b) $NiFe_{1.95}Sm_{0.05}O_4$ ferrites at room temperature at different doses

3.3 Vibrating sample magnetometer (VSM) measurements

Figure 10 shows room temperature hysteresis loops of $NiFe_{1.95}Gd_{0.05}O_4$ and $NiFe_{1.95}Sm_{0.05}O_4$ ferrites at different doses. The magnetic parameters; saturation magnetization (M_s), coercivity (H_c), and remanent magnetization (M_r) can be obtained from M–H curves. The values of these three magnetic parameters are listed in Table (4). In the case of the magnetic properties, the effect of the thermal neutron exposure is sharp and clear. Figure 11b presents the dose dependence of the coercivity. For $NiFe_{1.95}Gd_{0.05}O_4$, H_c decreases for GdZ2 and then it increases for GdZ8. whereas the saturation magnetization (M_s) increases slightly for GdZ2 and then strongly increases for GdZ8 (Figure 11c). Interestingly, this behavior is similar to the dose dependence of the particle size (D) and the microstrain. For $NiFe_{1.95}Sm_{0.05}O_4$, H_c initially increases for SmZ2, and then it decreases for SmZ8, whereas, M_s slightly decreases for SmZ2 and then strongly increases. In the same context, the increase of the saturation magnetization with increasing the dose is higher for $NiFe_{1.95}Gd_{0.05}O_4$ than that for $NiFe_{1.95}Sm_{0.05}O_4$. The squareness is affected by the magnetic anisotropy of the samples, particle size, shape, density, crystal defects, and synthesis methods [33]. For squareness ratio ≥ 0.5, the materials have a single magnetic domain structure, while for R^2 below 0.5, the materials have a multi magnetic domain structure. In the present case, the values of the squareness ratio are extremely small and below 0.5, and thus these materials have multi magnetic domains.

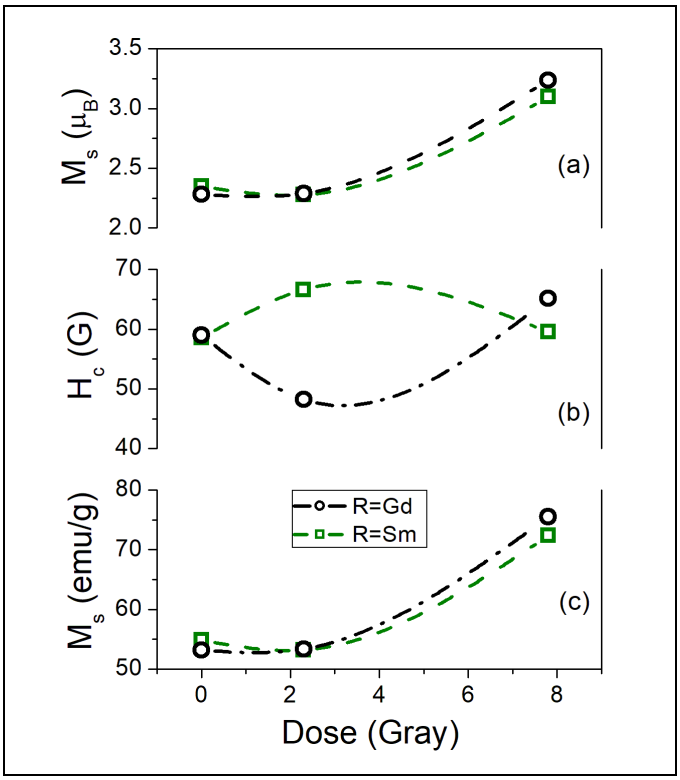

Fig. (11): The dose dependence of magnetic parameters of $NiFe_{1.95}Gd_{0.05}O_4$ and $NiFe_{1.95}Sm_{0.05}O_4$ ferrites: a) The saturation magnetization (M_s) in Bohr magneton unit b) The coercivity (H_c), c) The saturation magnetization (M_s)

Table (4): saturation magnetization (M_s), coercivity (H_c), remanent magnetization (M_r), and the squareness ratio ($R^2=M_r/M_s$) of $NiFe_{1.95}Gd_{0.05}O_4$ and $NiFe_{1.95}Sm_{0.05}O_4$ samples before and after thermal neutron exposure

	$NiFe_{1.95}Sm_{0.05}O_4$			$NiFe_{1.95}Gd_{0.05}O_4$		
	SmZ0	**SmZ2**	**SmZ8**	**GdZ0**	**GdZ2**	**GdZ8**
Ms (emu/g)	54.881	53.207	72.368	53.205	53.377	75.495
Hc (G)	58.533	66.613	59.538	58.997	48.225	65.141
Mr (emu/g)	2.5859	2.926	3.5336	2.5337	2.0726	4.1792
Mr/Ms	0.04712	0.05499	0.04883	0.04762	0.03883	0.05536
M_{obs} (μ_B)	2.34956	2.2779	3.09822	2.28109	2.28847	3.23675

To calculate the magnetic moment per formula unit in the Bohr magneton (μB), the following equation can be used [13]:

$$M_{obs} = \frac{M_S \times (molecular\ weight)}{5585} \qquad \textbf{(14)}$$

The values of the saturation magnetization are listed in Table (4) and Figure (11a). Néel's theory showed that the net magnetic moment of ferrite can be calculated as [34]:

$$M_{cal} = M_B - M_A \qquad \textbf{(15)}$$

The cation distribution $(Fe)_A[NiFe_{0.95}R_{0.05}]_BO_4$ is considered to calculate the magnetic moment of the tetrahedral and octahedral sites, M_A and M_B, respectively. The magnetic moment of Ni^{2+}, Fe^{3+}, Gd^{3+}, and Sm^{3+} ions are $2\mu_B$, $5\mu_B$, $7\mu_B$, and $5\mu_B$, respectively. The calculated magnetic moment for $NiFe_{1.95}Gd_{0.05}O_4$ is $2.1\mu_B$, whereas it is exactly $2\mu_B$ for $NiFe_{1.95}Sm_{0.05}O_4$. The experimental M_s values for $NiFe_{1.95}Gd_{0.05}O_4$ and $NiFe_{1.95}Sm_{0.05}O_4$ samples are higher than the values obtained from the Néel's model. In fact, Néel's model does not consider the effect of particle size, defects, and impurities on magnetic properties. In addition, the magnetic interactions in ferrites are strongly depending on the types of cations in the A and B-sites, distances, and angles between these cations. As mentioned before, XRD measurements suggest the decrease of lattice parameter by increasing the thermal neutron dose. By decreasing the lattice parameter, the distance between cations will also decrease and hence the magnetic interactions might increase. Even more, the thermal neutrons exposure increases the particle size and supports the incorporation of R^{3+} ions in the Ni-ferrite spinel lattice, which will logically affect the magnetic properties of these materials.

4. CONCLUSION

$NiR_{0.05}Fe_{1.95}O_4$ (R= Sm, and Gd) ferrite samples were prepared using the standard ceramic method. The rabbit system was used to irradiate the prepared samples with thermal neutrons doses of 2.3 and 7.8 Gy. The presence of the cubic spinel phase was confirmed by XRD diffraction patterns. In addition, a secondary phase of $RFeO_3$ with a minor amount was observed. By increasing the thermal neutron exposure dose, the peaks associated with this secondary phase are weakening. Exposing the samples to thermal neutron leads to the decrease of the lattice parameter, the increase of the particle size, and supports the incorporation of R^{3+} ions in the Ni-ferrite spinel lattice. $NiFe_{1.95}Gd_{0.05}O_4$ compound is more sensitive to thermal neutron exposure than the $NiFe_{1.95}Sm_{0.05}O_4$ compound due to the higher thermal neutrons capture cross section of Gd ions. The saturation magnetization increases with increasing the thermal neutron dose. Such an increase might be attributed to the decreased lattice parameter, which causes the shortening of distances between cations and hence strengthening the magnetic interaction.

REFERENCES

[1] S.I. Sharma, R.K. Kotnala, M. Singh, A. Kumar, P. Dhiman, V.P. Singh, K. Verma, G. Kumar, Structural, magnetic and Mössbauer studies of Nd-doped Mg-Mn ferrite nanoparticles. J. Magn. Magn. Mater. **44**, 77 (2017).

[2] Sucheta Sharma, K.S. Dayab, Sunil Sharma, K.M. Batood, M. Singh, Sol–gelauto combustion processed soft Z-type hexa nanoferrites for microwave antenna miniaturization. Ceram. Int. **41**, 7109 (2015).

[3] I. Sadiq, S. Naseem, M. Rana, M.N. Ashiq, I. Ali, Temperature dependent magnetic and microwave absorption properties of doubly substituted nano sized material. J. Magn. Magn. Mater. **385**, 236 (2015).

[4] P. Samoila, L. Sacarescu, A.I. Borhan, D. Timpu, M. Grigoras, N. Lupu, M. Zaltariov, V. Harabagiu, Magnetic properties of nanosized Gd doped Ni–Mn–Cr ferrites prepared using the sol–gel auto combustion technique. J. Magn. Magn. Mater. **378**, 92 (2015).

[5] S.R. Bhongale, H.R. Ingawale, T.J. Shinde, Kunal Pubby, S.B. Narang, P.N. Vasambekar, Nano-crystalline magnesium substituted cadmium ferrites as X-band microwave absorbers, J. Magn. Magn. Mater. **441**, 475 (2017).

[6] R. Rajesh Kanna, N. Lenin, K. Sakthipandi, M. Sivabharathy, Impact of lanthanum on structural, optical, dielectric and magnetic properties of $Mn_{1-x}Cu_xFe_{1.85}La_{0.15}O_4$ spinel nanoferrites, Ceram. Int. **43**, 15868 (2017).

[7] H. Huili, A. Mater, B. Grindi, G. Viau, A. Kouki, L.B. Tahar, Influence of the RE_2O_3 (RE = Y, Gd) and CaO nanoadditives on the electromagnetic properties of nanocrystalline $Co_{0.2}Ni_{0.3}Zn_{0.5}Fe_2O_4$, Arab. J. Chem. **12**, 489 (2017).

[8] K. Bibi, I. Ali, M.T. Farid, A. Mahmood, S.M. Ramay, K. Ali, Electric and dielectric properties of ytterbium substituted spinel Ferrites, J. Mater. Sci. Mater. Electron. **29**, 3744 (2018).

[9] M.T. Farid, I. Ahmad, M. Kanwal, G. Murtaza, I. Ali, S.A. Khan, The role of praseodymium substituted ions on electrical and magnetic properties of Mg spinel ferrites, J. Magn. Magn. Mater. **428**, 136 (2017).

[10] I. Sadiq, I. Ali, E. Rebrov, S. Naseem, M.N. Ashiq, M.U. Rana, Nanosized Ce–Zn substituted microwave absorber material for X-band applications. J. Magn. Magn. Mater. **370**, 25 (2014).

[11] M. Yehia, S.M. Ismail, A. Hashhash, Structural and magnetic studies of rare-earth substituted nickel ferrites. J. Supercond. Nov. Magn. **27**, 771 (2014).

[12] A. Goldman, Modem Ferrite Technology, 2nd edn. Springer, Berlin (2006).

[13] M. Yehia, Sh Labib, S.M. Ismail, Structural and magnetic properties of nano-$NiFe_2O_4$ prepared using green nanotechnology. Phys. B **446**, 49 (2014).

[14] S.S.R. Inbanathan, V. Vaithyanathan, J. Arout Chelvane, G. Markandeyulu, K. Kamala Bharathi, Mössbauer studies and enhanced electrical properties of R (R=Sm, Gd and Dy) doped Ni ferrite. J. Magn. Magn. Mater. **353**, 1 (2014).

[15] Dean, J.A.: Lange's Handbook of Chemistry. McGraw-Hill (1999).

[16] L. Ben Tahar, M. Artus, S. Ammar, L.S. Smiri, F. Herbst, M.-J. Vaulay, V. Richard, J.-M. Grenèche, F. Villain, F. Fiévet, Magnetic properties of $CoFe_{1.9}RE_{0.1}O_4$ nanoparticles (RE=La, Ce, Nd, Sm, Eu, Gd, Tb, Ho) prepared in polyol. J. Magn. Magn. Mater. **320**, 3242 (2008).

[17] M.A. Ahmed, S.I. El-dek, S.F. Mansour, N. Okasha, Modification of Mn nanoferrite physical properties by gamma, neutron, and laser irradiations Solid State Sciences, **13**, 1180-1186 (2011).

[18] I.A. Ali, Gehan Y. Mohamed, A. Azzam, A.A. Sattar, Determination of concentrations of Fe, Mg, and Zn in some ferrite samples using neutron activation analysis and X-ray fluorescence techniques, Applied Radiation and Isotopes **122**, 63-67 (2017).

[19] International Committee on Radiological Protection (ICRP), Conversion Coefficients for use in Radiological Protection against External Radiation (1997).

[20] N. Xoubi, Neutrons and Gamma-Ray Dose Calculations in Subcritical Reactor Facility Using MCNP, Atoms **4**, 20 (2016).

[21] N. Rezlescu, E. Rezlescu, C. Pasnicu, M.L. Craus, Induced size effects of Gd^{3+} ions doping on structural and magnetic properties of Ni-Zn ferrite nanoparticles. J. Phys. Condens. Matter **6**, 5707 (1994).

[22] E.E. Sileo, S.E. Jacobo, Gadolinium-Nickel ferrites prepared from metal citrates precursors. Phys. B **354**, 241 (2004).

[23] S.I. Ahmad, S.A. Ansari, D.R. Kumar, Structural, morphological, magnetic properties and cation distribution of Ce and Sm co-substituted nano crystalline cobalt ferrite. Mater. Chem. Phys. 208, 248 (2018)

[24] S.F. Mughabghab, Thermal neutron capture cross sections resonance integrals and g-factors. IAEA: **INDC(NDS)-440**, 22 (2003).

[25] T.M. Ali, S.M. Ismail, S.F. Mansour, M.A. Abdo, M. Yehia, Physical properties of Al-doped cobalt nanoferrite prepared by citrate–nitrate auto combustion method. J Mater Sci: Mater Electron **32**, 3092 (2021).

[26] J.M. Thompson, Infrared Spectroscopy (Pan Stanford Publishing Pte. Ltd., Singapore, (2018).

[27] V. Rathod, A.V. Anupama, R. Vijaya Kumar, V.M. Jali, B. Sahoo, Correlated vibrations of the tetrahedral and octahedral complexes and splitting of the absorption bands in FTIR spectra of Li–Zn ferrites. Vib. Spectrosc. **92**, 267 (2017).

[28] B.J. Yang, H. Shin, H.K. Lee, H. Kim, A combined molecular dynamics/ micromechanics/ finite element approach for multiscale constitutive modeling of nanocomposites with interface effects. Appl. Phys. Lett. **103**, 241903 (2013).

[29] A. Rais, K. Taibi, A. Addou, A. Zanoun, Y. Al-Douri, Copper substitution effect on the structural properties of nickel ferrites. Ceram. Int. **40**, 14413 (2014).

[30] K.B. Modi, M.K. Rangolia, M.C. Chhantbar, H.H. Joshi, Study of infrared spectroscopy and elastic properties of fine and coarse grained nickel–cadmium ferrites. J. Mater. Sci. **41**, 7308 (2006).

[31] M.S. Gumaan, Chromium improvements on the mechanical performance of a rapidly solidified eutectic Sn–Ag alloy. J. Mater. Sci. Mater. Electron. **31**, 10731 (2020).

[32] M. Deepty, Ch. Srinivas, E. Kumar, N. Ranjith Mohan, C.L. Krisha Prajapat, T.V. Chandrasekhar Rao, S.S. Meena, A.K. Verma, D.L. Sastry, XRD, EDX, FTIR and ESR spectroscopic studies of co-precipitated Mn-substituted Zn-ferrite nanoparticles. Ceram. Int. **45**, 8037 (2019).

[33] Ati, Ali A. Othaman, Zulkafli Samavati, Alireza, Influence of cobalt on structural and magnetic properties of nickel ferrite nanoparticles, Journal of Molecular Structure **1052**, 177 (2013).

[34] S.M. Ismail, M. Yehia, S.S. Ata-Allah, Influence of Zinc Doping on the Structural and Magnetic Properties of Ni-Ga-Sm Polycrystalline Ferrites. J. Supercond. Nov. Magn. **28**, 2875 (2015).